Hindawi Publishing Corporation
Modelling and Simulation in Engineering
Volume 2014, Article ID 381760, 20 pages
http://dx.doi.org/10.1155/2014/381760

Research Article

Instantaneous Power Theory with Fourier and Optimal Predictive Controller Design for Shunt Active Power Filter

Suksan Tiyarachakun, Kongpol Areerak, and Kongpan Areerak

School of Electrical Engineering, Institute of Engineering, Suranaree University of Technology, Nakhon Ratchasima 30000, Thailand

Correspondence should be addressed to Kongpol Areerak; kongpol@sut.ac.th

Received 24 March 2014; Revised 22 May 2014; Accepted 22 May 2014; Published 24 June 2014

Academic Editor: Aiguo Song

This paper presents a novel harmonic identification algorithm of shunt active power filter for balanced and unbalanced three-phase systems based on the instantaneous power theory called instantaneous power theory with Fourier. Moreover, the optimal design of predictive current controller using an artificial intelligence technique called adaptive Tabu search is also proposed in the paper. These enhancements of the identification and current control parts are the aim of the good performance for shunt active power filter. The good results for harmonic mitigation using the proposed ideas in the paper are confirmed by the intensive simulation using SPS in SIMULINK. The simulation results show that the enhanced shunt active power filter can provide the minimum %THD (Total Harmonic Distortion) of source currents and unity power factor after compensation. In addition, the %THD also follows the IEEE Std.519-1992.

1. Introduction

Power systems connected nonlinear loads can generate the harmonics into the systems. These harmonics cause a lot of disadvantages such as loss in transmission lines and electric devices, protective device failures, and short-life electronic equipment in the system [1–3]. Therefore, it is very important to reduce or eliminate the harmonics in the system. It is well known that the harmonic elimination via a shunt active power filter (SAPF) [4] provides higher efficiency and more flexibility compared with a passive power filter. There are four main parts (part A–D) for using the SAPF to mitigate the harmonics in the system as shown in Figure 1.

The Part A is the harmonic identification method to calculate the reference currents for SAPF. There are many methods for harmonic identification such as an instantaneous power theory (PQ) [5, 6], a synchronous reference frame (SRF) [7], a synchronous detection (SD) [8], a sliding window Fourier analysis (SWFA) [9], an a-b-c reference frame [10], and a DQ-axis with Fourier (DQF) [11].

The Part B is the SAPF structure. There are two types of SAPF topology such as the voltage source inverter (VSI) [12, 13] and the current source inverter (CSI) [13, 14] with six IGBTs. The VSI topology is used in the paper because this topology is simple and provides the good performance for harmonic elimination.

The Part C is the control technique to control the compensating current of SAPF. There are several techniques to control the compensating current injection such as a hysteresis control [15, 16], a PWM technique with PI controller [15, 16], a sliding mode control [17, 18], a predictive control [19–21], a fuzzy logic control [22, 23], and a neural network control [16].

The Part D is the last part for harmonic elimination using SAPF. This part is the DC bus voltage control of SAPF. There are various types of the voltage control to regulate the DC bus voltage such as PI controller [24, 25], fuzzy logic controller [26], and RST controller [24]. In the paper, the PI controller is used to control the DC bus voltage.

The aim of this paper is the minimum %THD of source currents after compensation via SAPF. The Part A and Part C are the significant parts to achieve the minimum %THD. Therefore, the performances of Part A and Part C must be improved. In Part A, the PQ method is selected for improvement because this algorithm is simple and because of unity power factor confirmation after compensation. The

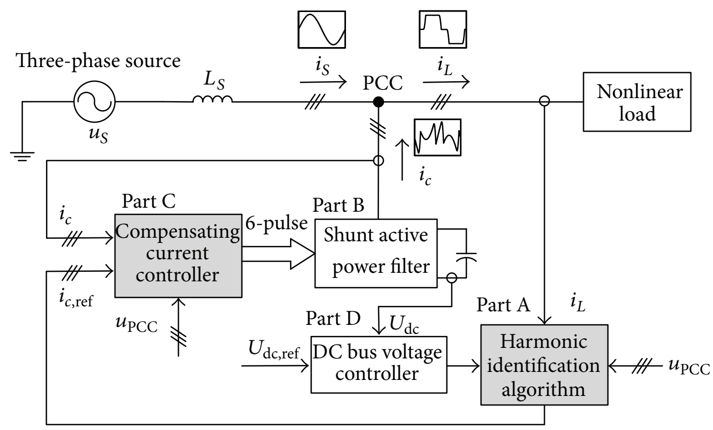

Figure 1: The harmonic elimination system via shunt active power filter.

conventional PQ method uses the analog filter to draw the harmonic component of the instantaneous active power from fundamental component. This approach has an error to calculate the harmonic component. Therefore, the SWFA technique is applied to draw the harmonic component for harmonic identification improvement. The PQ with SWFA method called an instantaneous power theory with Fourier (PQF) algorithm is presented in the paper. The details of the PQF algorithm and the performance comparison between the PQ and PQF for balanced and unbalanced systems are explained in Section 2.

There are many advantages for minimum %THD of source currents such as minimum loss in transmission lines and electric devices, more accuracy of protective devices, and long-life electronic equipments. Therefore, the minimum %THD of source currents is necessary. Normally, many research works [13, 14, 19, 21, 24, 27, 28] focus on how to reduce %THD of the system to follow the IEEE Std.519-1992 but do not care about the minimum %THD. The improvement of harmonic identification part (Part A) is not sufficient to achieve the minimum %THD nearly global solution. Therefore, the development of the compensating current controller (Part C) is the additional approach to present in the paper. The predictive current control is selected to improvement in Part C because this controller compensates the delay incurred through digital control implementation and provides good static and dynamic performances. The conventional predictive current control uses the first-order Lagrange equation to approximate the predicted reference currents. Presently, it is well known that there are many artificial intelligence (AI) techniques to apply for the optimization problems in the engineering researches such as the multiobjective harmony search (MOHS) [29], artificial bee colony (ABC) [30, 31], competition particle swarm optimization (CPSO) [32], genetic algorithm (GA) [33], and adaptive Tabu search (ATS) [34–47]. The ATS method is developed by Puangdownreong et al. in 2002 [34]. In order to perform its effectiveness, the ATS has tested against several well-known benchmark functions, that is, Bohachevsky, Rastrigin, Shekel's foxholds, Shubert, and Schwefel functions [42–46]. Moreover, the convergence property of the ATS has been proved to assure that it can reach the optimal solution within finite search time [42–47]. Thus, the ATS is selected to design the predictive current controller in the paper. The ATS approach can provide the good performance to control the compensating currents injection and guarantees the optimal solution for searching. The review of the conventional predictive current control on dq-axis is described in Section 3. The ATS method is briefly explained in Section 4. In Section 5, the optimal design of the predictive current controller using the ATS method is fully shown. Finally, Section 6 concludes and discusses the advantages of the proposed ideas to enhance the performance of SAPF. In the paper, the improvement of the harmonic identification and current controller design parts of SAPF is called the enhanced shunt active power filter (ESAPF).

2. Instantaneous Power Theory with Fourier

The harmonic identification algorithm for reference current calculations is very important for the harmonic mitigation with SAPF. The perfect reference currents are necessary for an enhanced shunt active power filter or ESAPF. Therefore, a novel algorithm to calculate the reference currents of ESAPF is presented in this section. This algorithm is called the instantaneous power theory with Fourier algorithm or PQF. The PQF algorithm is developed from the instantaneous power theory (PQ). The PQ algorithm is firstly public in 1983 by Akagi et al. [5]. The performance comparison between the PQ and PQF algorithm is discussed in this section. The performance indices for comparison are %THD of source currents and power factor after compensation. The harmonic mitigation systems with the ideal shunt active power filter for balanced and unbalanced systems as shown in Figures 2 and 7, respectively. In Figure 2, the three-phase bridge rectifier feeding resistive and inductive loads ($R = 130\,\Omega$ and $L = 4$ H) behaves as a nonlinear load into the balanced three-phase system. In Figure 7, the three single-phase bridge rectifiers with different RL loads are the nonlinear load for an unbalanced three-phase system. The ideal current source is used to represent the ideal shunt active power filter to perfectly inject the compensating currents (i_{ca}, i_{cb}, i_{cc}) into the power system

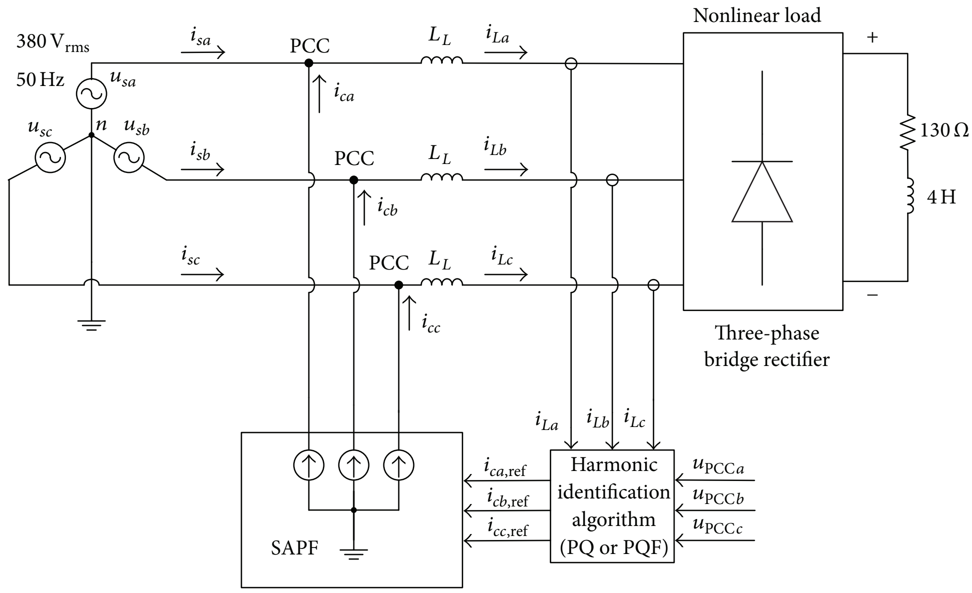

FIGURE 2: The balanced power system with ideal shunt active power filter.

at the point of common coupling (PCC). The compensating currents are equal to the reference currents ($i_{ca,\text{ref}}, i_{cb,\text{ref}}, i_{cc,\text{ref}}$) because of using the ideal current source model for SAPF. The block diagram to calculate the reference currents using PQ and PQF algorithm for balanced and unbalanced three-phase systems is depicted in Figure 3. Figure 3 shows that there are six steps to calculate the reference currents.

Step 1. Three-phase voltages at PCC point ($u_{\text{PCC}a}$, $u_{\text{PCC}b}$, $u_{\text{PCC}c}$) are transformed to $\alpha\beta 0$ frame ($u_{\text{PCC}\alpha}, u_{\text{PCC}\beta}, u_{\text{PCC}0}$) using equation in block number 1.

Step 2. Transform the three-phase load currents (i_{La}, i_{Lb}, i_{Lc}) to the $\alpha\beta 0$ frame ($i_{L\alpha}, i_{L\beta}, i_{L0}$) by the block number 2.

Step 3. Calculate the instantaneous active power (p_L) and reactive power (q_L) on the $\alpha\beta 0$ frame in the block number 3. The p_L from the block number 3 consists of two components, the fundamental component ($\overline{p}_L$) and the harmonic component ($\widetilde{p}_L$).

Step 4. Draw the $\widetilde{p}_L$ from the p_L. For PQ algorithm, the separation of the fundamental and harmonic components uses the analog filter (high-pass filter: HPF). In this paper, the cutoff frequencies of HPF for balanced and unbalanced systems are equal to 280 Hz and 50 Hz, respectively. On the other hand, the sliding window Fourier analysis (SWFA) is used to separate these components for PQF algorithm. In this step, the method to separate the fundamental and harmonic components is the different point between the PQ and PQF algorithm. After to draw the $\widetilde{p}_L$ from p_L, the reference active power (p_c) can be obtained from subtracting between $\widetilde{p}_L$ and p_{dc} (output of the PI controller in the DC bus voltage control part). In the paper, the reference reactive power is set equal to q_L because of the unity power factor after compensation.

Step 5. Calculate the reference currents on the $\alpha\beta 0$ frame ($i_{c\alpha,\text{ref}}, i_{c\beta,\text{ref}}, i_{c0,\text{ref}}$) by the equation of block number 5.

Step 6. Calculate the three-phase reference currents ($i_{ca,\text{ref}}$, $i_{cb,\text{ref}}, i_{cc,\text{ref}}$) for SAPF using the equation of block number 6.

From Figure 3, it can be seen that the zero sequence calculations are necessary for unbalanced three-phase system. For the balanced system, the zero sequence quantities are equal to zero.

The SWFA technique for PQF algorithm uses the Fourier series of active power as shown in (1). From this equation, A_{0p}, A_{hp}, and B_{hp} are the Fourier series coefficients, T_s is the sampling interval, k is time index, h is the harmonic order, and ω is the angular fundamental frequency of the system. The fundamental component (or DC component) of active power is represented by A_{0p} coefficient as shown in (2). The A_{hp} coefficient in (1) can be calculated by (3). The A_{0p} coefficient or DC component can be calculated by substitute $h = 0$ in (3) as shown in (4). The N_0 and N in (3) and (4) are the starting point for computing and the total number of sampled point in one cycle, respectively. The calculation of A_{0p} in the first period can be calculated using (4) so as to achieve the initial value for the PQF algorithm. For the next period, the A_{0p} can be calculated by (5) in which this approach is called SWFA [9]. The SWFA approach can be summarized in Figure 4:

$$p_L(kT_s) = \frac{A_{0p}}{2} + \sum_{h=1}^{\infty} \left[A_{hp} \cos(h\omega kT_s) + B_{hp} \sin(h\omega kT_s) \right], \tag{1}$$

$$\overline{p}_L(kT_s) = \frac{A_{0p}}{2}, \tag{2}$$

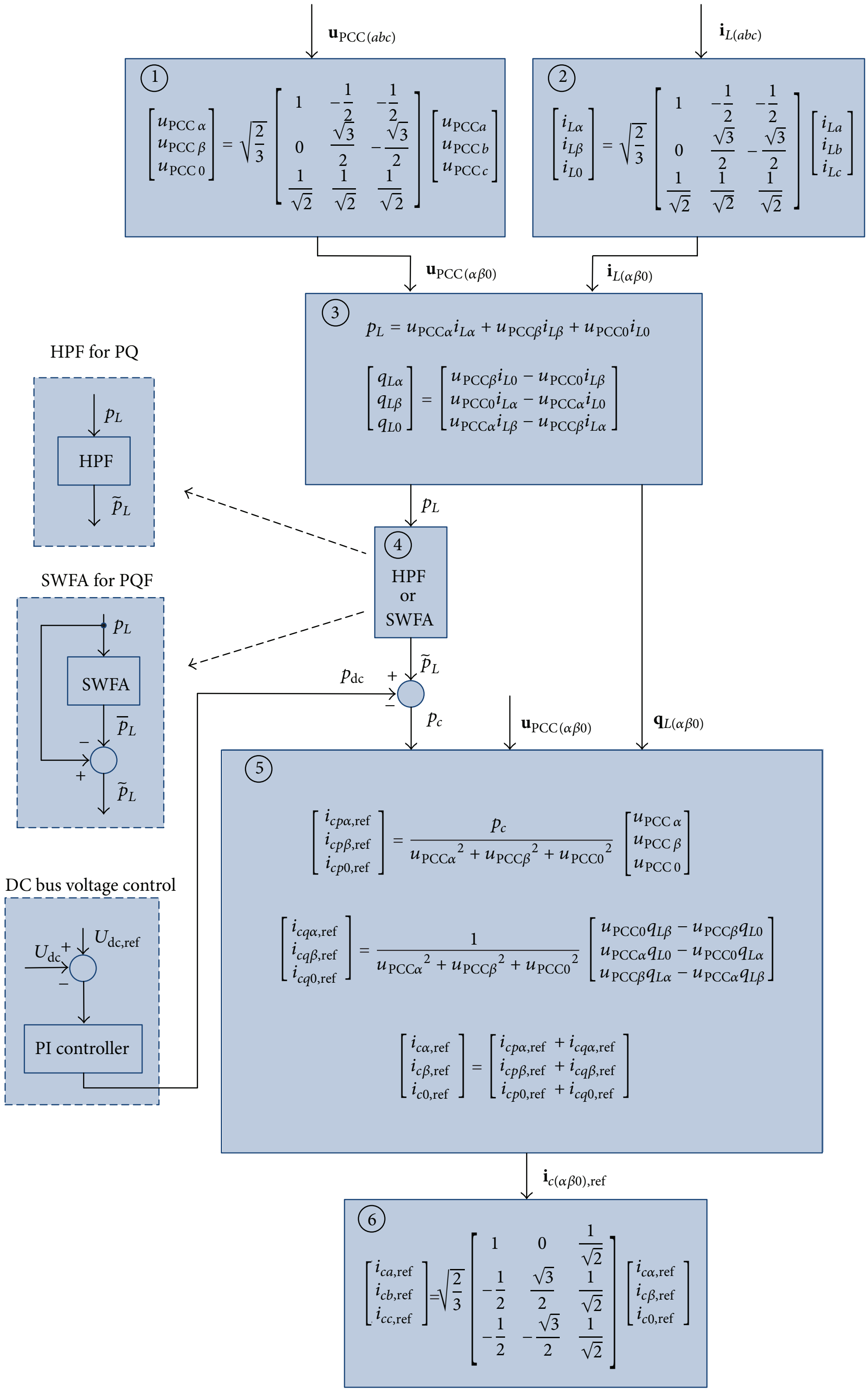

FIGURE 3: The block diagram of PQ and PQF algorithms.

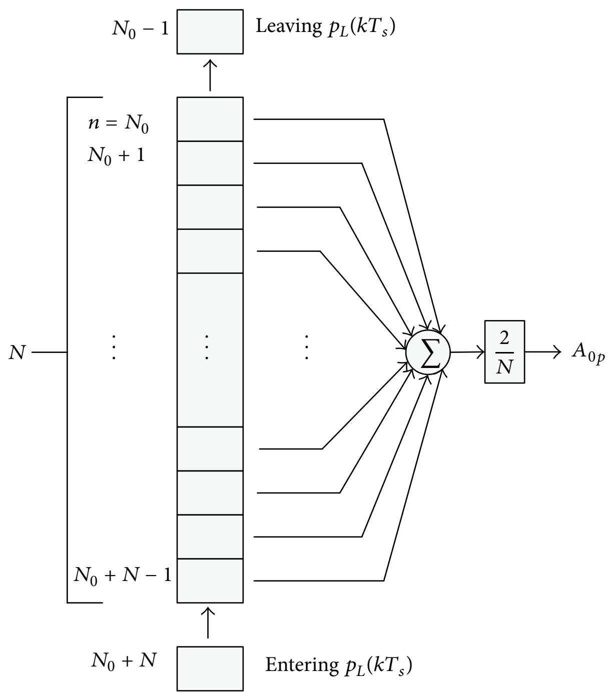

Figure 4: The flow chart of the SWFA approach.

Table 1: The performance comparison between the PQ and PQF algorithms for balanced system.

Harmonic identification algorithm	Before compensation				After compensation			
	$\%\mathrm{THD}_{i,av}$	$\mathrm{pf}_{\mathrm{disp}}$	$\mathrm{pf}_{\mathrm{dist}}$	pf	$\%\mathrm{THD}_{i,av}$	$\mathrm{pf}_{\mathrm{disp}}$	$\mathrm{pf}_{\mathrm{dist}}$	pf
PQ	24.48	0.98	0.97	0.95	0.95	1	1	1
PQF					0.04	1	1	1

$$A_{hp} = \frac{2}{N} \sum_{n=N_0}^{N_0+N-1} p_L(nT_s) \cos(nh\omega T_s), \tag{3}$$

$$A_{0p} = \frac{2}{N} \sum_{n=N_0}^{N_0+N-1} p_L(nT_s), \tag{4}$$

$$\begin{aligned} A_{0p}^{(\mathrm{new})} = A_{0p}^{(\mathrm{old})} &- \frac{2}{N} p_L\left[(N_0 - 1) T_s\right] \\ &+ \frac{2}{N} p_L\left[(N_0 + N) T_s\right]. \end{aligned} \tag{5}$$

The simulation results of the performance comparison between the PQ and PQF algorithms for the balanced system in Figure 2 with $L_L = 10\,\mathrm{mH}$ are addressed in Table 1. The cutoff frequency of HPF for PQ method is set to 280 Hz. The average %THD of source currents ($\%\mathrm{THD}_{i,\mathrm{av}}$) and the power factor after compensation (pf) are the performance indices for the comparison. The $\%\mathrm{THD}_{\mathrm{av}}$ and pf can be calculated by (6) and (8), respectively. The %THD of source currents in each phase ($\%\mathrm{THD}_{i,k}$) can be calculated by (7). The fundamental and harmonic (order n) values in (7) are denoted by subscript 1 and n, respectively. The $\mathrm{pf}_{\mathrm{disp}}$ and $\mathrm{pf}_{\mathrm{dist}}$ in (8) are the displacement and distortion power factors in which these values can be calculated by (9) and (10), respectively:

$$\%\mathrm{THD}_{i,\mathrm{av}} = \sqrt{\frac{\sum_{k=a,b,c} \%\mathrm{THD}_{i,k}^2}{3}}, \tag{6}$$

$$\%\mathrm{THD}_{i,k} = \frac{\sqrt{\sum_{n=2}^{\infty} I_{n,k}^2}}{I_{1,k}} \times 100\%, \tag{7}$$

$$\mathrm{pf} = \frac{P}{S} = \mathrm{pf}_{\mathrm{disp}} \times \mathrm{pf}_{\mathrm{dist}}, \tag{8}$$

$$\mathrm{pf}_{\mathrm{disp}} = \frac{P}{S_1}, \tag{9}$$

$$\mathrm{pf}_{\mathrm{disp}} = \frac{1}{\sqrt{1 + \mathrm{THD}_u^2} \times \sqrt{1 + \mathrm{THD}_i^2}}. \tag{10}$$

The results from Table 1 show that the PQF algorithm can provide the best performance in term of $\%\mathrm{THD}_{i,\mathrm{av}}$. From Table 1, the $\%\mathrm{THD}_{i,\mathrm{av}}$ of the source currents before compensation is equal to 24.48% in which this value is extremely greater than the IEEE std.519-1992. The source current waveforms before compensation (i_{sa}, i_{sb}, i_{sc}) are highly

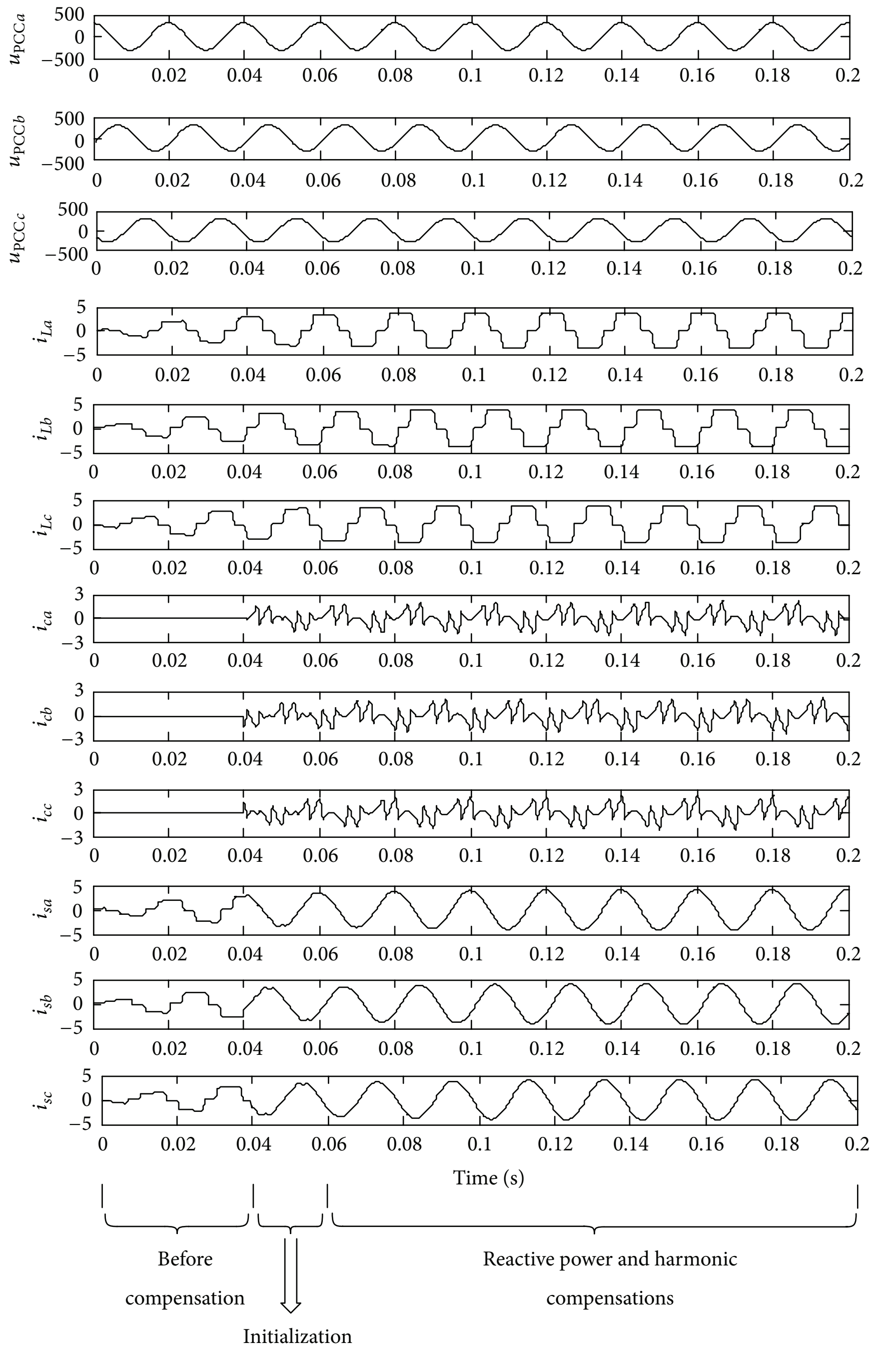

Figure 5: The simulation results using PQF algorithm for ideal shunt active power filter with balanced system.

Table 2: The error of instantaneous active power for harmonic component calculation.

Frequency (Hz)	$\tilde{p}_{L,\mathrm{act}}$	$\tilde{p}_{L,\mathrm{PQ}}$	$\tilde{p}_{L,\mathrm{PQF}}$	error (%) PQ	error (%) PQF
300	173.3885	171.3400	173.3175	1.18	0.04
600	59.5549	59.3269	59.4681	0.38	0.15
900	27.7095	27.6630	27.6932	0.17	0.06
1200	13.9776	14.0036	14.0208	0.19	0.31
		E_{tot}		1.92	0.56

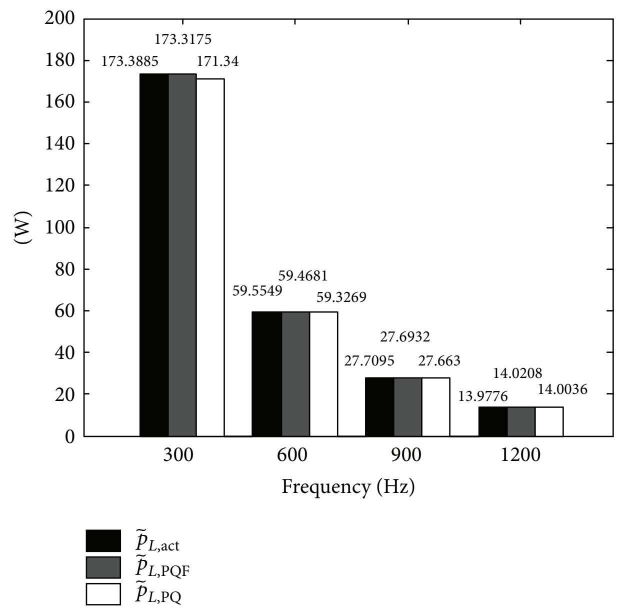

Figure 6: The spectrum of instantaneous active power for harmonic components.

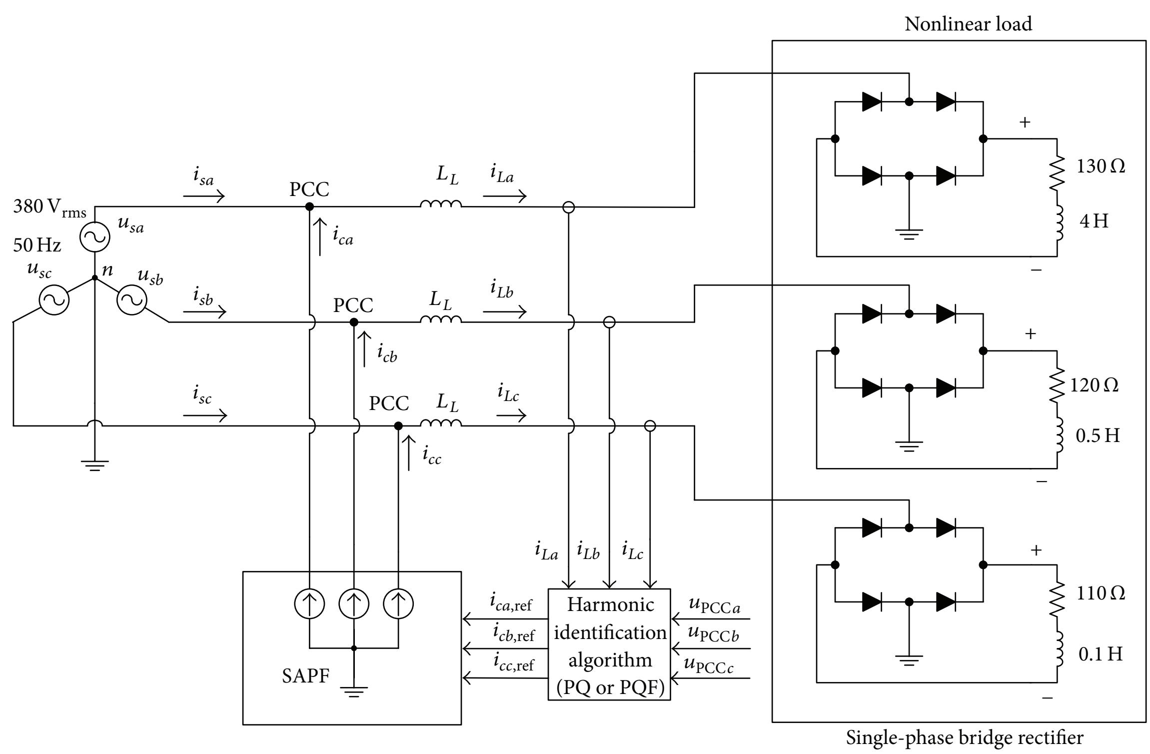

Figure 7: The unbalanced power system with ideal shunt active power filter.

distorted as shown in Figure 5. These waveforms are equal to the load currents (i_{La}, i_{Lb}, i_{Lc}) before compensation because the SAPF is not connected to the system. From Figure 5, the compensating currents (i_{ca}, i_{cb}, i_{cc}) from SAPF are injected into the system at $t = 0.04$ s. For $t = 0.04$–0.06 s, the compensation is nonperfect because this interval is used for initial of SWFA algorithm. The SWFA algorithm is the main approach for PQF method. After $t = 0.06$ s, the SAPF generates the perfectly compensating currents into the system (reactive power and harmonic compensations). From Figure 5 ($t \geq 0.06$ s), it can be seen that the source currents after compensation are nearly sinusoidal waveforms. The %THD$_{i,\mathrm{av}}$ of these currents is equal to 0.95 and 0.04 for PQ and PQF, respectively as shown in Table 1. These values

Table 3: The performance comparison between the PQ and PQF algorithms for unbalanced system.

Harmonic identification algorithm	%THD$_{i,a}$	%THD$_{i,b}$	%THD$_{i,c}$	%THD$_{i,av}$	i_{sa} (rms)	i_{sb} (rms)	i_{sc} (rms)	%unbalance
				Before compensation				
	42.84	32.75	8.51	31.52	1.46	1.61	1.92	15.43
				After compensation				
PQ	0.62	0.49	0.68	0.60	1.55	1.56	1.55	0.43
PQF	0.01	0.01	0.01	0.01	1.55	1.55	1.55	0

are satisfied under IEEE std.519-1992. Moreover, the power factor after compensation is unity, while before compensation the power factor is equal to 0.95.

From Figure 3, the different point between the PQ and PQF algorithm is the method to separate the fundamental and harmonic components. Therefore, the accurate instantaneous active power for harmonic component ($\tilde{p}_L$) is the main objective to identify the harmonic currents of the system. The spectrum comparison of the $\tilde{p}_L$ values calculated by PQF and PQ algorithms is shown in Figure 6. The $\tilde{p}_{L,\text{act}}$ is the spectrum of the instantaneous harmonic active power calculated by FFT approach from MATLAB programming. The $\tilde{p}_{L,\text{PQF}}$ and $\tilde{p}_{L,\text{PQ}}$ are calculated by PQF and PQ algorithms, respectively. From Figure 6, it can be seen that the $\tilde{p}_{L,\text{PQF}}$ value calculated by PQF algorithm is nearly the same as the $\tilde{p}_{L,\text{act}}$ value. The errors between the $\tilde{p}_L$ values calculated by PQF and PQ algorithms compared with the $\tilde{p}_{L,\text{act}}$ value are shown in Table 2. In the paper, the authors focus on the total error (E_{tot}) for the performance comparison between the PQ and PQF algorithms. From Table 2, the E_{tot} from PQF algorithm (0.56%) is less than the PQ algorithm (1.56%). Therefore, the PQF algorithm is the perfect method to calculate the reference currents for ESAPF.

The simulation results of the performance comparison between the PQ and PQF algorithms for the unbalanced system in Figure 7 are addressed in Table 3. The results from Table 3 show that the PQF algorithm can provide the best performance in term of %THD$_{i,\text{av}}$ and %unbalance after compensation. The %unbalance in this table can be calculated by (11). From Table 3, the %THD$_{i,\text{av}}$ and %unbalance of source currents before compensation are equal to 31.52% and 15.43%, respectively. The waveforms of source current (i_{sa}, i_{sb}, i_{sc}) before compensation (t = 0–0.04 s) are extremely distorted and unbalanced as depicted in Figure 8. For t = 0.04–0.06 s, this interval is the initial calculation for PQF algorithm using a SWFA technique. For $t \geq 0.06$ s, the PQF algorithm can completely eliminate the harmonic currents and balance the amplitude and phase of source currents after compensation. The %THD$_{i,\text{av}}$ of these currents are equal to 0.60 and 0.01 for PQ and PQF, respectively, as given in Table 3. The %unbalance after compensation using PQ and PQF algorithms is equal to 0.43 and 0, respectively. It means that the source currents after compensation are perfectly balanced using the PQF algorithm compared with the %unbalance before compensation (15.43%). From the simulation results of the balanced and unbalanced system, the PQF algorithm is the perfect method to calculate the reference currents for ESAPF. In the future works, the positive sequence detection is added to the PQF algorithm for the harmonic current elimination in the distorted and unbalanced voltage systems:

$$\%\text{unbalance} = \frac{|\text{maximum current deviation from average rms current}|}{\text{average rms current}} \times 100\%. \tag{11}$$

3. Predictive Current Control on dq-Axis

In this section, the predictive current control for SAPF with balanced three-phase system is proposed. The predictive current control technique is applied to control the injection of compensating currents with SAPF as shown in Figure 9. The voltage source inverter with six IGBTs is the SAPF topology in the paper. The PQF algorithm described in the previous section is used to identify the harmonic currents in the system. The three-phase bridge rectifier feeding resistive and inductive loads behaves as a nonlinear load into the power system. The predictive current control is the suitable technique for a digital control [21]. The equivalent circuit in Figure 10 is used to derive the relationship equation between the SAPF output voltages ($\mathbf{u}_{(abc)}$) and the voltages at PCC point ($\mathbf{u}_{\text{PCC}(abc)}$) as given in (12). The compensating currents or active filter currents are represented by $\mathbf{i}_{c(abc)}$. The discrete form of (12) can be represented by (13) and T_{sc} is the sampling time of the controller:

$$\mathbf{u}_{(abc)} = L_f\left(\frac{d\mathbf{i}_{c(abc)}}{dt}\right) + \mathbf{u}_{\text{PCC}(abc)}, \tag{12}$$

$$\mathbf{u}_{(abc)}(k) = \frac{L_f}{T_{sc}}\left[\mathbf{i}_{c(abc)}(k+1) - \mathbf{i}_{c(abc)}(k)\right] + \mathbf{u}_{\text{PCC}(abc)}(k). \tag{13}$$

The concept of the reference currents prediction is shown in Figure 11. From this figure, the three-phase reference current at time instants $t(k)$ and $t(k+1)$ is denoted by $\mathbf{i}_{c(abc),\text{ref}}(k)$ and $\mathbf{i}_{c(abc),\text{ref}}(k+1)$, respectively. The predicted three-phase reference currents ($\mathbf{i}_{cp(abc),\text{ref}}(k+1)$) for the next sampling period are calculated by (14). The predicted currents ($\mathbf{i}_{cp(abc),\text{ref}}(k+1)$) are equal to the reference currents ($\mathbf{i}_{c(abc),\text{ref}}(k+1)$) at time instant $t(k+1)$. The a_0 and a_1 are the

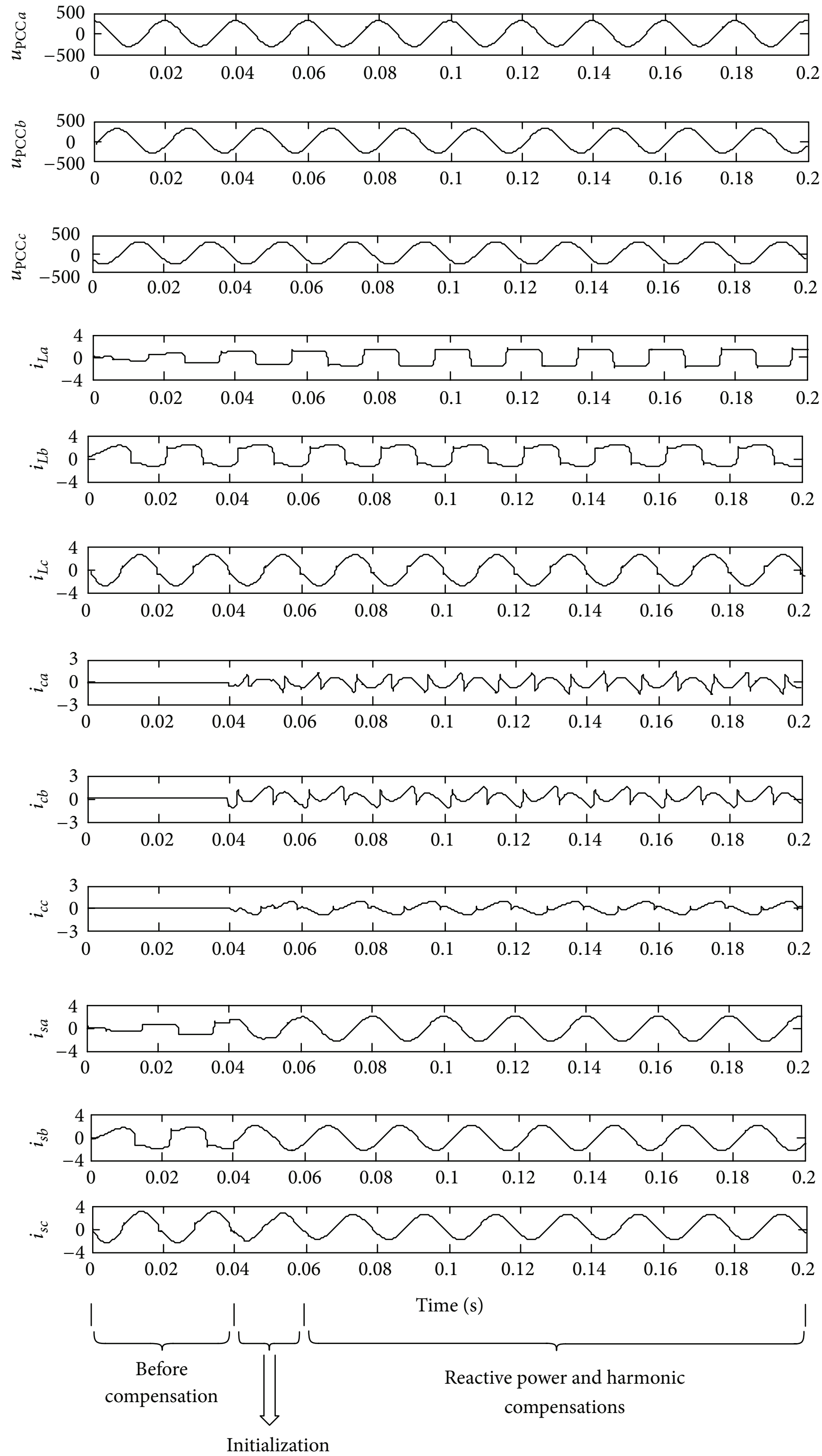

FIGURE 8: The simulation results using PQF algorithm for ideal shunt active power filter with unbalanced system.

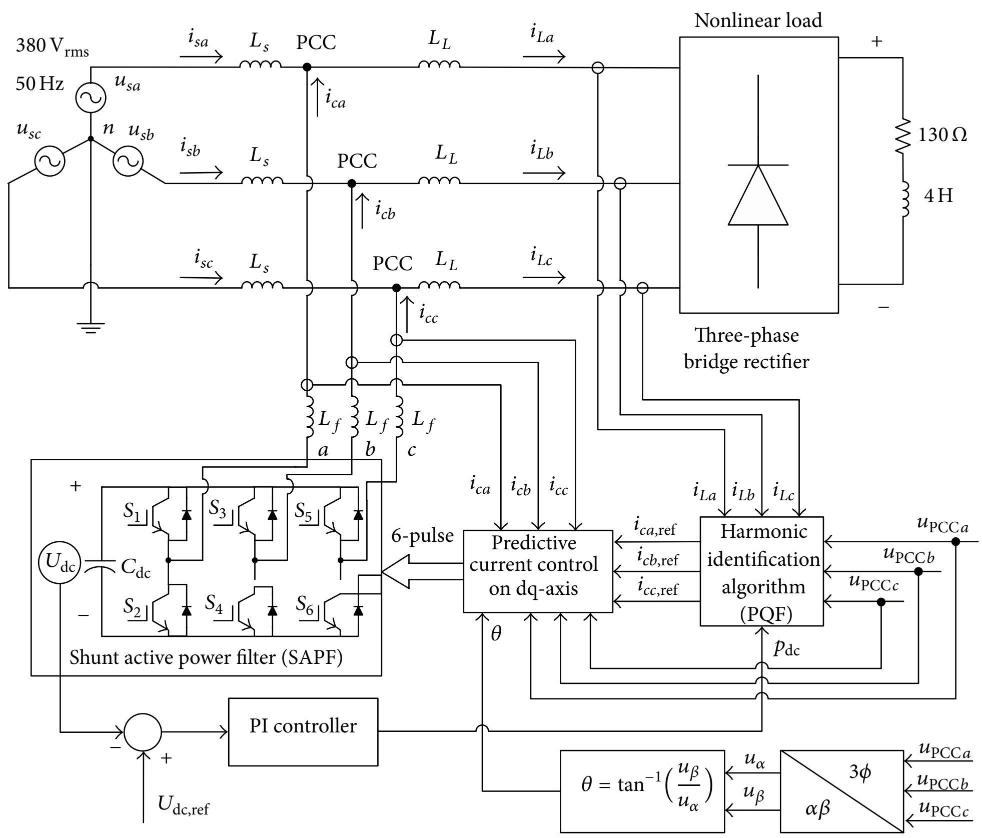

Figure 9: The balanced power system with the predictive current control of SAPF.

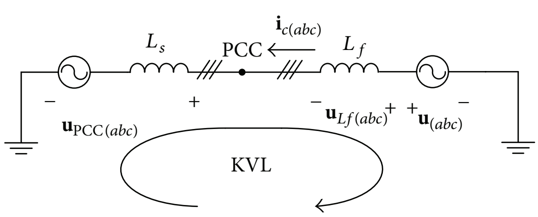

Figure 10: The equivalent circuit of the SAPF connected with the voltages at the PCC point.

coefficients of the first-order in Lagrange equation ($a_0 = 2$, $a_1 = -1$). The Lagrange equation is used to approximate the reference currents one sampling instant ahead by using known values from a few previous sampling instant. The output voltages of SAPF are assumed to be constant during the one sampling time:

$$\mathbf{i}_{cp(abc),\mathrm{ref}}(k+1) = a_0\mathbf{i}_{c(abc),\mathrm{ref}}(k) + a_1\mathbf{i}_{c(abc),\mathrm{ref}}(k-1). \quad (14)$$

Equations (12)–(14) are used for three-phase values. In the paper, the predictive current control is applied on dq-axis. Therefore, the equations to calculate the output voltages of SAPF and the predicted reference currents on dq-axis are shown in (15) and (16), respectively. The Park's transformation is used to transform the three-phase quantities to dq-axis quantities. The overall procedure to calculate the output voltages of SAPF using predictive current control is depicted in Figure 12. The output voltages of SAPF are used to generate the six-pulse of IGBTs ($S_1 - S_6$) via the PWM technique:

$$\begin{aligned}\mathbf{u}_{(\mathrm{dq})}(k) &= \frac{L_f}{T_{sc}}\left[\mathbf{i}_{cp(\mathrm{dq}),\mathrm{ref}}(k+1) - \mathbf{i}_{c(\mathrm{dq})}(k)\right] \\ &\quad + L_f\omega\begin{bmatrix}0 & -1\\ 1 & 0\end{bmatrix}\mathbf{i}_{c(\mathrm{dq})}(k) + \mathbf{u}_{\mathrm{PCC(dq)}}(k),\end{aligned} \quad (15)$$

$$\mathbf{i}_{cp(\mathrm{dq}),\mathrm{ref}}(k+1) = a_0\mathbf{i}_{c(\mathrm{dq}),\mathrm{ref}}(k) + a_1\mathbf{i}_{c(\mathrm{dq}),\mathrm{ref}}(k-1). \quad (16)$$

The simulation results of the system with $L_s = 0.01$ mH and $L_L = 10$ mH in Figure 9 are shown in Table 4. The inductor (L_f), capacitor (C_{dc}), and the DC bus reference voltage ($U_{\mathrm{dc,ref}}$) of SAPF are equal to 39 mH, 250 μF, and 750 V, respectively. The PI controller is applied to regulate the DC bus voltage ($K_p = 3$, $K_I = 24$). The %THD$_{i,\mathrm{av}}$ of source currents (i_{sa}, i_{sb}, i_{sc}) before compensation is equal to 24.91%,

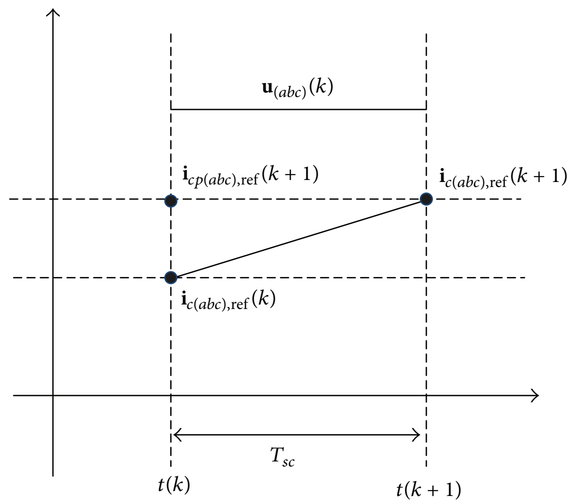

FIGURE 11: The concept of predictive current control.

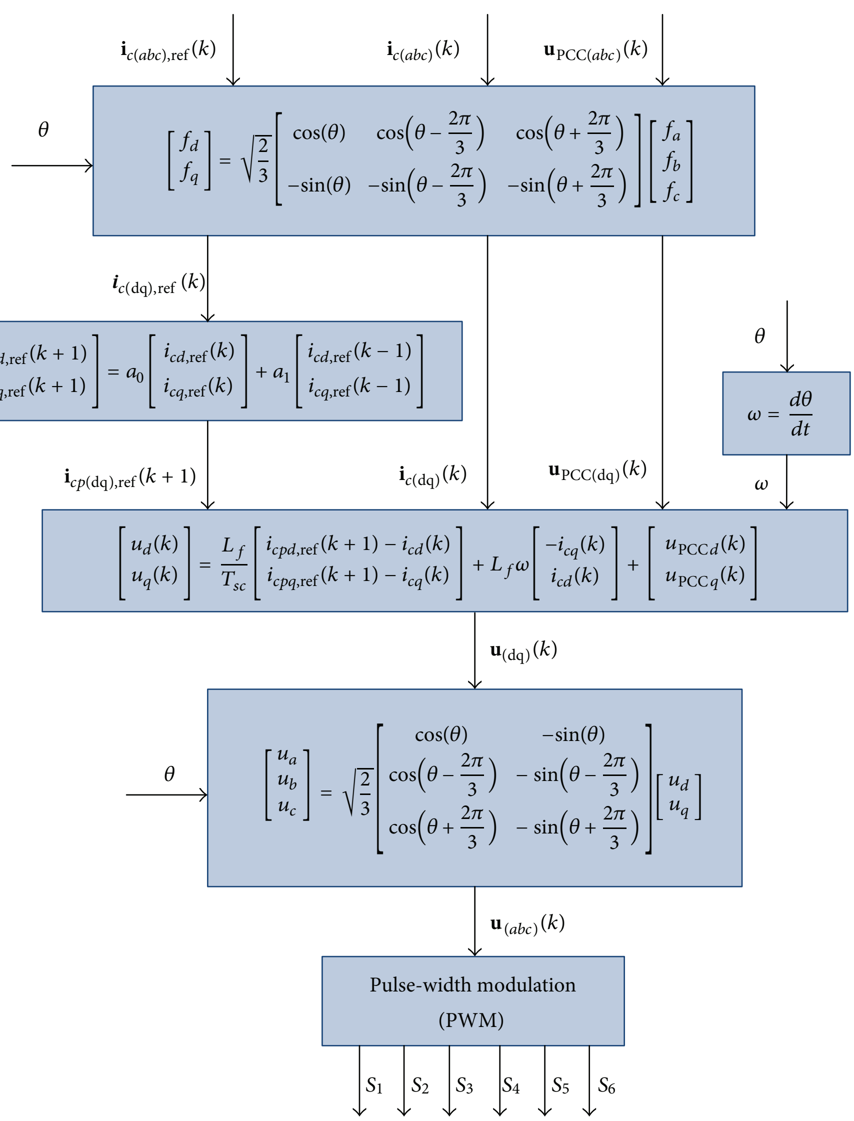

FIGURE 12: The overall procedure of the predictive current control for SAPF.

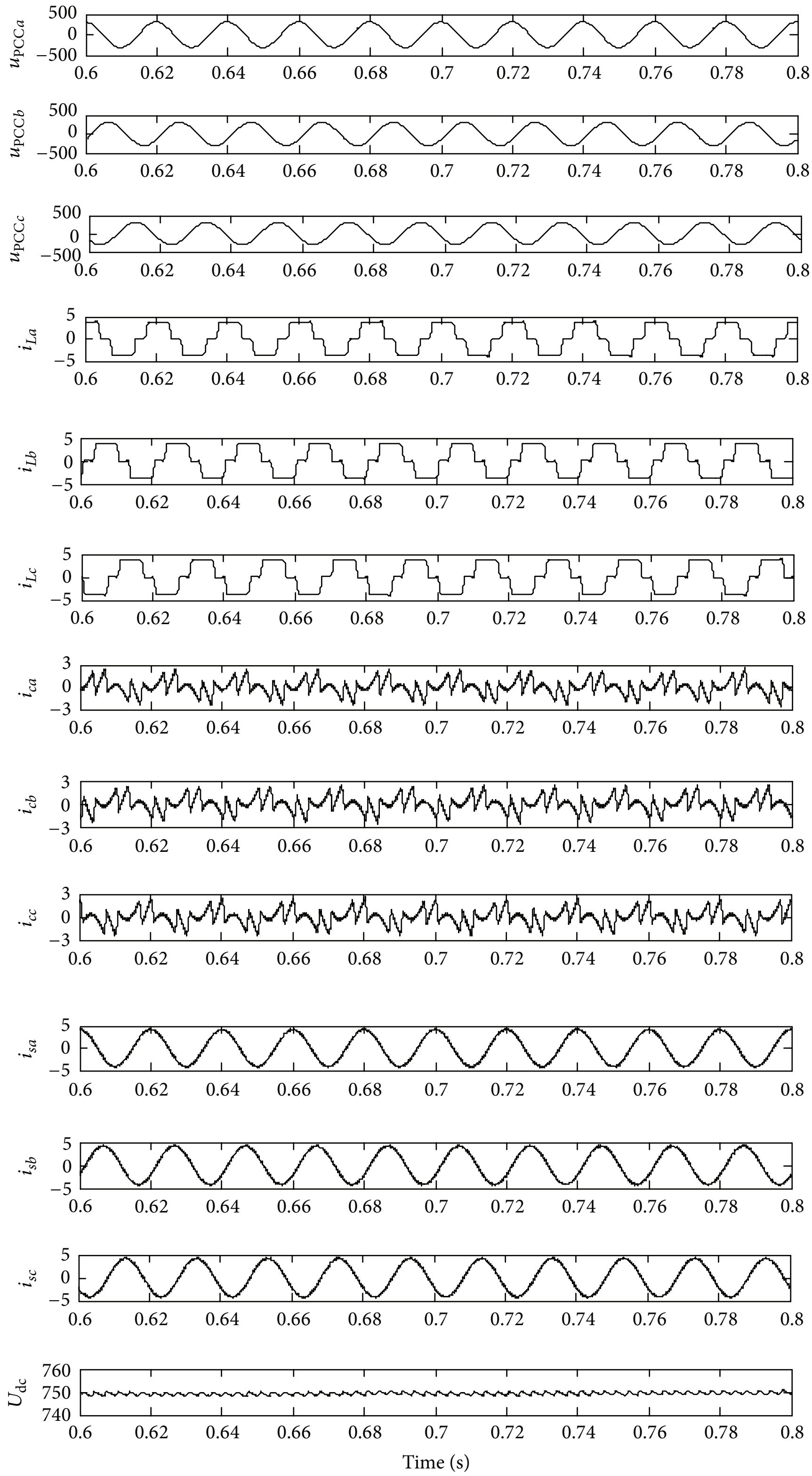

FIGURE 13: The simulation results using first-order Lagrange equation.

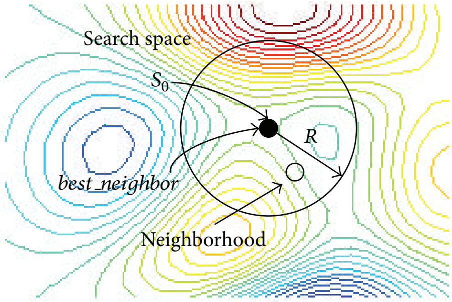

FIGURE 14: Random S_0 in search space.

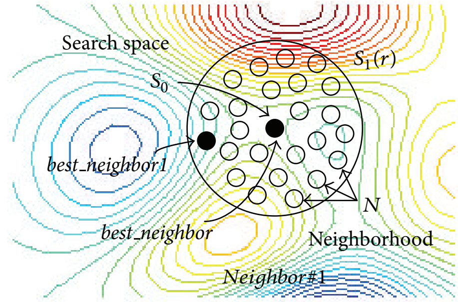

FIGURE 15: Neighborhood around S_0.

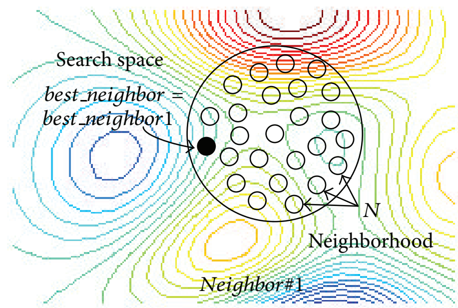

FIGURE 16: Assign a new *best_neighbor.*

while %THD$_{i,\mathrm{av}}$ after compensation with predictive current control technique using first-order Lagrange equation is 1.40%. The current and voltage waveforms of the system in Figure 9 are depicted in Figure 13.

In Figure 13, the compensating currents (i_{ca}, i_{cb}, i_{cc}) from SAPF are injected into the system. The source currents before compensation are highly distorted waveform (%THD$_{i,\mathrm{av}}$ = 24.91%). After compensation, the source currents are nearly sinusoidal waveform (%THD$_{i,\mathrm{av}}$ = 1.40%). Moreover, the PI controller can regulate the DC bus voltage to 750 V. The design of the predictive current control using the adaptive Tabu search (ATS) method without the first-order Lagrange equation is explained in Section 5.

4. Review of ATS Algorithm

The adaptive Tabu search or ATS method [34–47] is used to design the predictive current controller to minimize %THD$_{i,\mathrm{av}}$ of source currents after compensation. The review of the ATS algorithm is described in this section. The ATS algorithm is improved from the Tabu Search (TS) method by adding two mechanisms, namely, back-tracking and adaptive search radius. The modified version of the TS method has been named the adaptive tabu search of ATS. The ATS algorithm can be outlined as follows.

Step 1. Initialize the tabu list TL and *Count* (a number of search round) = 0.

Step 2. Randomly select the initial solution S_0 from the search space. S_0 is set as a local minimum and S_0 = *best_neighbor* as shown in Figure 14.

Step 3. Update Count then randomly select N new solutions from the search space of a radius R. Let $S_1(r)$ be a set containing N solutions as shown in Figure 15.

Step 4. Compute the cost value of each member of $S_1(r)$. Then, choose the best solution and assign it as *best_neighbor1* (see Figure 15).

Step 5. If *best_neighbor1* < *best_neighbor*, then keep best_neighbor in the TL, set *best_neighbor* = *best_neighbor1* (see Figure 16), and set S_0 = *best_neighbor* (see Figure 17). Otherwise, put *best_neighbor1* in the TL instead.

Step 6. Evaluate the termination criteria (TC) and the aspiration criteria (AC). If Count *MAX_Count* (the maximum number allowance of search round), stop the searching process. The current best solution is the overall best solution. Otherwise, go back to *Step* 2 and start the searching process again until all criteria is satisfied (see Figure 18).

The back-tracking process allows the system to go back and look up the previous solutions in TL. The better solution is then chosen among the current and the previous solutions. Figure 19 illustrates details of the back-tracking process.

Given this new search space to explore, the search process is likely to have more chances of escaping from the local optimum. The back-tracking mechanism can be added into *Step* 5 to improve the searching performance.

The adaptive radius process as depicted in Figure 20 decreases the search area during the searching process. The adaptive radius mechanism has been developed to adjust the radius (R) by using the cost of the solution. The criterion for adapting the search radius is given as follows:

$$\mathrm{radius}_{\mathrm{new}} = \frac{\mathrm{radius}_{\mathrm{old}}}{\mathrm{DF}}, \quad (17)$$

where DF is a decreasing factor. The adaptive search radius mechanism can be added into the end of *Step* 6 to improve the searching performance. The more details of ATS algorithm can be found in [34–47].

Table 4: The simulation results.

Case	Parameters		$\%THD_{i,av}$	
	a_0	a_1	Before compensation	After compensation
First-order Lagrange equation	2	−1	24.91	1.40
Designed by ATS method	2.85	−1.86		0.96

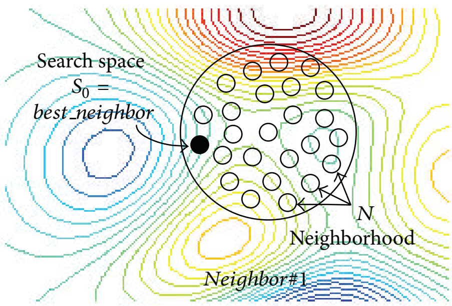

Figure 17: Assign a new S_0.

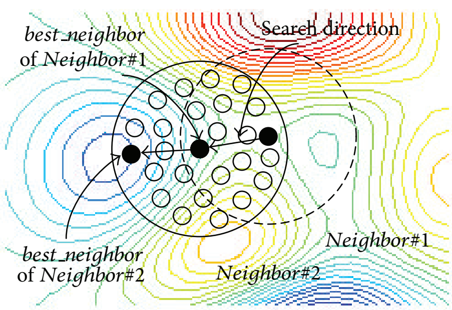

Figure 18: Searching process in the next iteration.

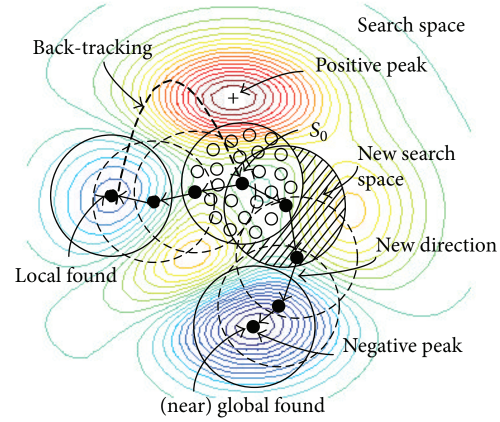

Figure 19: Back-tracking in ATS algorithm.

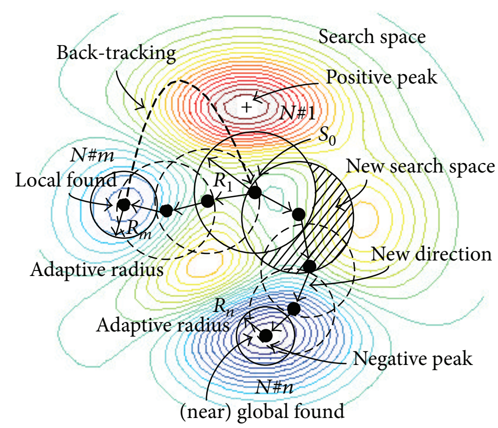

Figure 20: ATS algorithm with adaptive search radius mechanism.

5. Optimal Design of Predictive Current Controller

In Section 3, the predicted currents are calculated by the first-order Lagrange equation in (14) with $a_0 = 2$, $a_1 = -1$. In this section, the ATS algorithm is applied to determine the appropriate coefficients (a_0 and a_1) of (14) for $\%THD_{i,av}$ minimization. The block diagram to explain how to search the a_0 and a_1 coefficients using the ATS algorithm is depicted in Figure 21. As can be seen in Figure 21, the ATS will try to search the best coefficients of (14) to achieve the minimum $\%THD_{i,av}$. The cost value of the ATS searching is $\%THD_{i,av}$ of source currents. In each searching round, the $\%THD_{i,av}$ value can be calculated by M-file programming, while the actual three-phase source currents are obtained from Simulink as shown in Figure 21.

In the ATS process, the a_0 and a_1 coefficients are adjusted to achieve the best solution; here it is the minimum $\%THD_{i,av}$. The convergence of the $\%THD_{i,av}$ value is shown in Figure 22. It can be seen that $\%THD_{i,av}$ can converge to the minimum point. The $\%THD_{i,av}$ in Figure 22 can escape the local point to get the better solution because of the back tracking approach in the ATS algorithm. Moreover, the convergences of a_0 and a_1 coefficient values are shown in Figures 23 and 24, respectively. In the paper, the maximum of searching iteration for ATS is set to 300 rounds, number of initial solution = 400, number of N neighborhood = 40, initial radius of search space = 0.4, and decreasing factor value (DF) = 1.2. From the ATS searching results, a_0 and a_1 coefficients are equal to 2.85 and −1.86, respectively. The simulation results of the system in Figure 9 with the predictive current controller designed by ATS algorithm are shown in Figure 25. The source currents after compensation are nearly sinusoidal waveform and $\%THD_{i,av}$ of these currents are equal to 0.96 as shown in Table 4. From the results, the predictive current controller designed by ATS algorithm can provide the smaller $\%THD_{i,av}$ compared with the current controller using first-order Lagrange equation. The results show that the ATS approach is very useful and more convenient for the optimal design of predictive current control in SAPF system. The

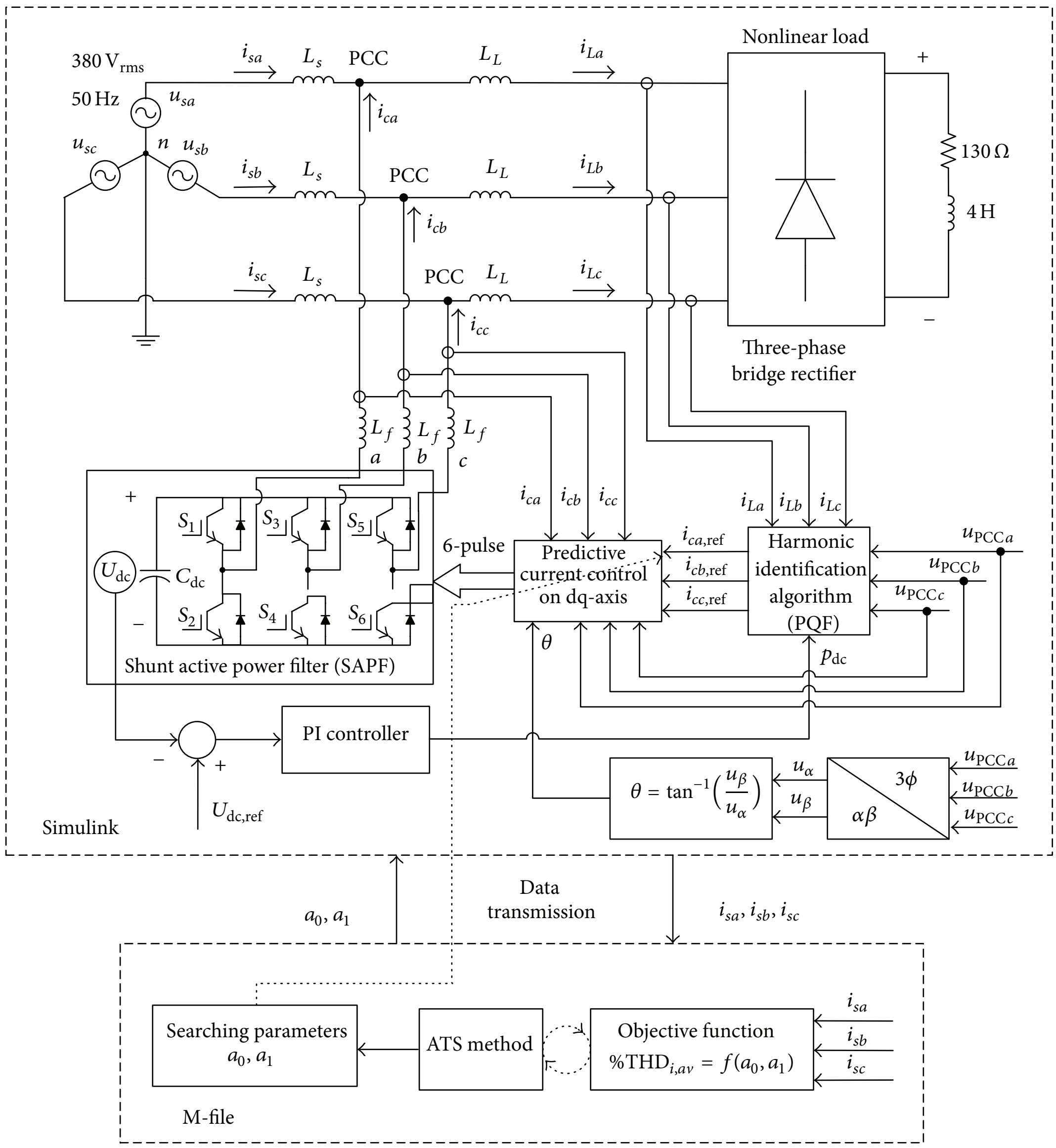

Figure 21: The design of predictive current controller using ATS algorithm.

simulation results for harmonic currents elimination with dynamic load changing are shown in Figure 26. From this figure, the load of three-phase bridge rectifier is suddenly changed at $t = 1$ s. After load changing, the SAPF can also mitigate the harmonic currents and the DC bus voltage controller can also regulate the DC voltage equal to 750 V.

6. Conclusion

The instantaneous power theory with Fourier or PQF algorithm is proposed in the paper. The performance comparison between the PQ and PQF is also presented by the simulation via the software package. The simulation results show that the PQF algorithm can provide the accurate reference currents for a shunt active power filter. Moreover, the optimal design of predictive current controller by ATS method is shown in the paper. This controller can provide the best performance of harmonic elimination compared with the conventional predictive current control. The shunt active power filter using the PQF algorithm to identify the harmonic and using the compensating current controller designed by ATS method is called the enhanced shunt active power filter (ESAPF). The results from simulation confirm that the ESAPF provides the minimum %THD and unity power factor of power supply at PCC point.

List of Symbols

i_{ca}, i_{cb}, i_{cc}: the three-phase compensating currents

$u_{\text{PCC}a}, u_{\text{PCC}b}, u_{\text{PCC}c}$: the three-phase voltages at PCC point

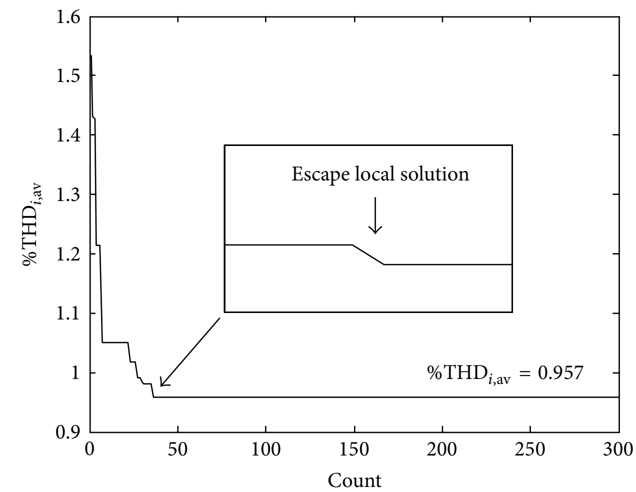

Figure 22: The convergence of the %THD$_{i,\text{av}}$.

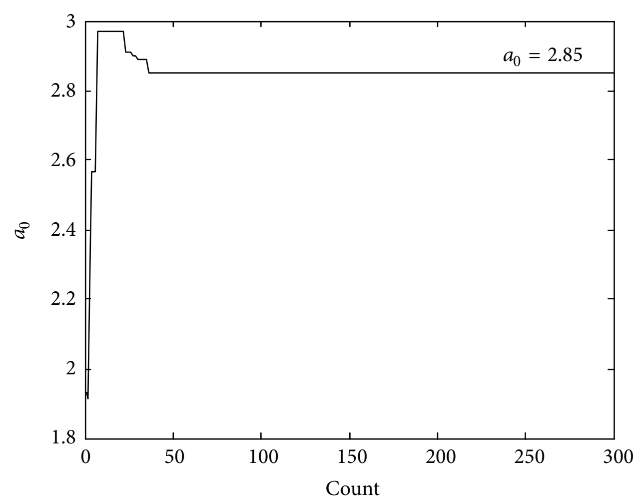

Figure 23: The convergence of a_0 coefficient.

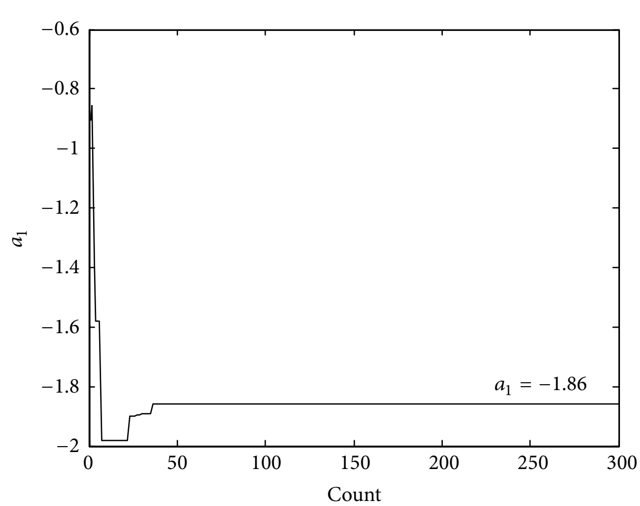

Figure 24: The convergence of a_1 coefficient.

$u_{\text{PCC}\alpha}, u_{\text{PCC}\beta}, u_{\text{PCC}0}$:	the voltages at PCC point on $\alpha\beta0$ frame
i_{La}, i_{Lb}, i_{Lc}:	the three-phase load currents
$i_{L\alpha}, i_{L\beta}, i_{L0}$:	the load currents on $\alpha\beta0$ frame
p_L and q_L:	the instantaneous active power and reactive power
$\overline{p}_L$:	the fundamental component of instantaneous active power
$\widetilde{p}_L$:	the harmonic component of instantaneous active power
p_c:	the reference active power
$i_{c\alpha,\text{ref}}, i_{c\beta,\text{ref}}, i_{c0,\text{ref}}$:	the reference currents on $\alpha\beta0$ frame
$i_{ca,\text{ref}}, i_{cb,\text{ref}}, i_{cc,\text{ref}}$:	the three-phase reference currents
A_{0p}, A_{hp}, B_{hp}:	the Fourier series coefficients
T_s:	the sampling interval
k:	time index
h:	the harmonic order
ω:	the angular fundamental frequency of the system
N_0:	the starting point for computing
N:	the total number of sampled point in one cycle
%THD$_{i,\text{av}}$:	the average %THD of source currents
pf:	the power factor after compensation
pf$_{\text{disp}}$ and pf$_{\text{dist}}$:	the displacement and distortion power factors
i_{sa}, i_{sb}, i_{sc}:	the three-phase source currents
$\widetilde{p}_{L,\text{act}}$:	the instantaneous harmonic active power calculated by FFT
$\widetilde{p}_{L,\text{PQ}}$:	the instantaneous harmonic active power calculated by PQ
$\widetilde{p}_{L,\text{PQF}}$:	the instantaneous harmonic active power calculated by PQF
$\mathbf{u}_{(abc)}$:	the SAPF output voltages
$\mathbf{u}_{Lf(abc)}$:	the inductive filter voltages
$\mathbf{u}_{\text{PCC}(abc)}$:	the voltages at PCC point
$\mathbf{i}_{c(abc)}$:	the compensating currents
T_{sc}:	the sampling time of the controller
$i_{cp(abc),\text{ref}}(k+1)$:	the predicted three-phase reference currents
$i_{c(abc),\text{ref}}(k)$ and $i_{c(abc),\text{ref}}(k+1)$:	the three-phase reference current at time instants $t(k)$ and $t(k+1)$
a_0, a_1:	the coefficients of the first-order in Lagrange
$U_{\text{dc,ref}}$:	the DC bus reference voltage of SAPF
U_{dc}:	the DC bus voltage of SAPF
Count:	a number of search round
MAX_Count:	the maximum number allowance of search round
DF:	a decreasing factor.

Conflict of Interests

The authors declare that there is no conflict of interests regarding the publication of this paper.

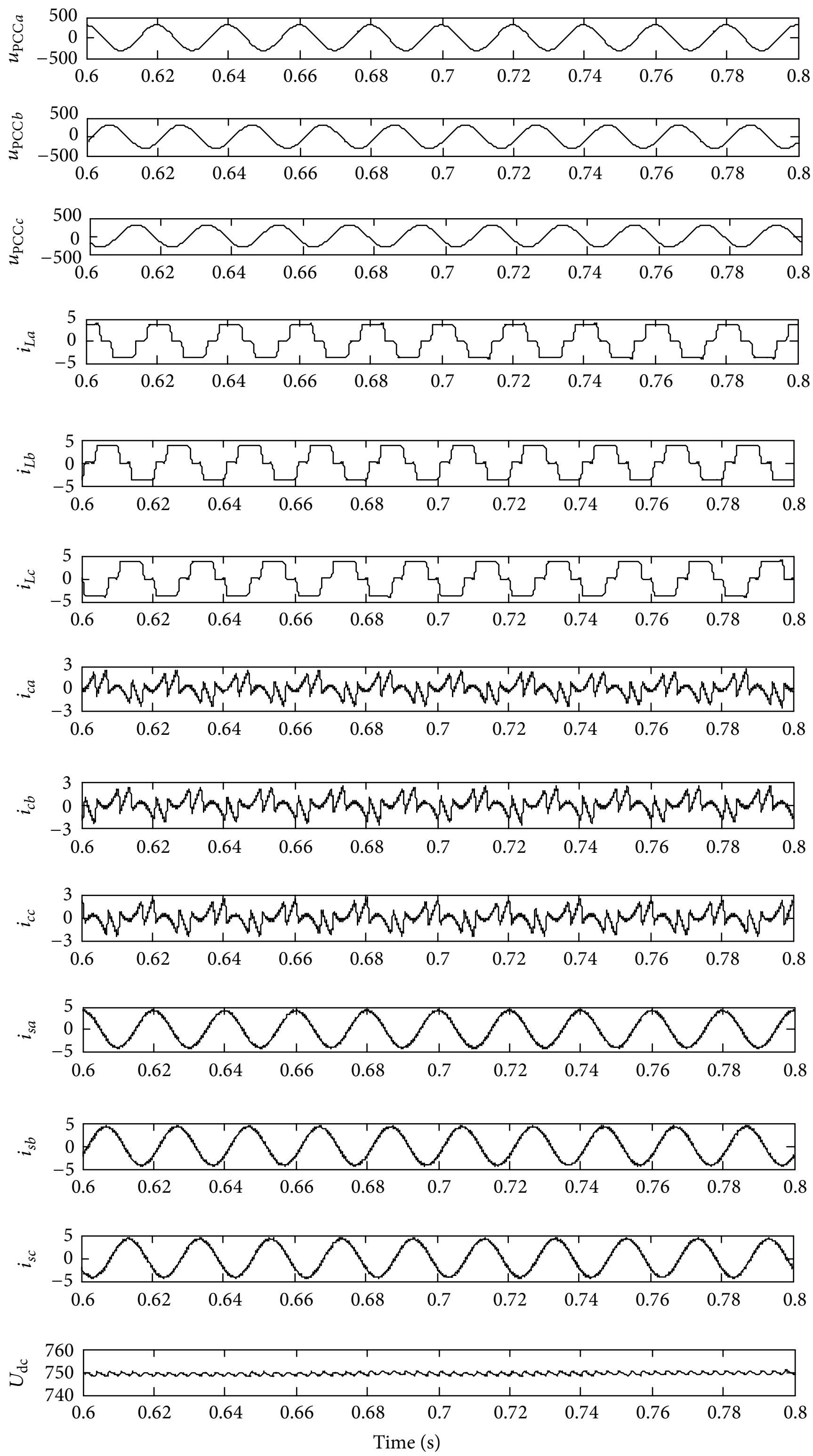

FIGURE 25: The simulation results using predictive current control designed by ATS.

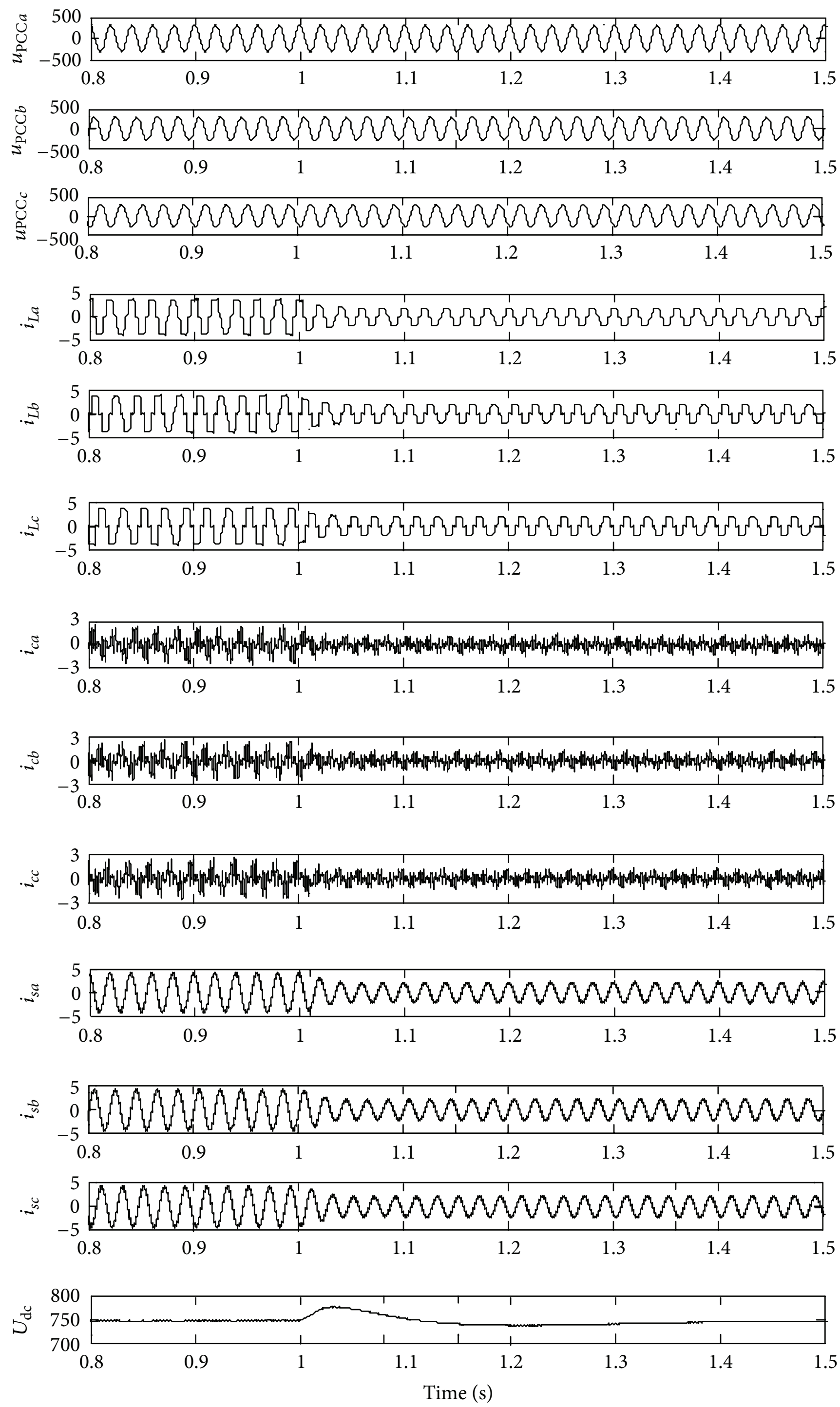

FIGURE 26: The simulation results for dynamic load changing.

Acknowledgments

This work was supported by Suranaree University of Technology (SUT) and by the office of the Higher Education Commission under NRU project of Thailand. The author would like to thank Associate Professor Dr. Deacha Puangdownreong for providing the useful information of ATS algorithm.

References

[1] J. M. Ho and C. C. Liu, "The effects of harmonics on differential relay for a transformer," in *Proceedings of the 16th International Conference and Exhibition on Electricity Distribution, IEE Conference Publication no. 482*, vol. 2, Amsterdam, The Netherlands, 2001.

[2] D. E. Rice, "Adjustable speed drive and power rectifier harmonics–their effect on power systems components," *IEEE*

Transactions on Industry Applications, vol. 22, no. 1, pp. 161–177, 1986.

[3] V. E. Wagner, J. C. Balda, D. C. Griffith et al., "Effects of harmonics on equipment," *IEEE Transactions on Power Delivery*, vol. 8, no. 2, pp. 672–680, 1993.

[4] T. Thomas, K. Haddad, G. Joós, and A. Jaafari, "Design and performance of active power filters," *IEEE Industry Applications Magazine*, vol. 4, no. 5, pp. 38–46, 1998.

[5] H. Akagi, Y. Kanazawa, and A. Nabae, "Instantaneous reactive power compensators comprising switching devices without energy storage components," *IEEE Transactions on Industry Applications*, vol. 20, no. 3, pp. 625–630, 1984.

[6] R. S. Herrera and P. Salmerón, "Present point of view about the instantaneous reactive power theory," *IET Power Electronics*, vol. 2, no. 5, pp. 484–495, 2009.

[7] M. Takeda, K. Ikeda, A. Teramoto, and T. Aritsuka, "Harmonic current and reactive power compensation with an active filter," in *Proceedings of the 19th Annual IEEE Power Electronics Specialists Conference (PESC '88)*, vol. 2, pp. 1174–1179, Kyoto, Japan, 1988.

[8] C. L. Chen, C. E. Lin, and C. L. Huang, "The reference active source current for active power filter in an unbalanced three-phase power system via the synchronous detection method," in *Proceedings of the 10th Anniversary IEEE Instrumentation and Measurement Technology Conference (IMTC '94)*, vol. 2, pp. 502–505, Hamamatsu, Japan, May 1994.

[9] M. El-Habrouk and M. K. Darwish, "Design and implementation of a modified Fourier analysis harmonic current computation technique for power active filter using DSPs," *IEE Proceedings—Electric Power Applications*, vol. 148, no. 1, pp. 21–28.

[10] G. W. Chang, S. K. Chen, and M. Chu, "An efficient a-b-c reference frame-based compensation strategy for three-phase active power filter control," *Electric Power Systems Research*, vol. 60, no. 3, pp. 161–166, 2002.

[11] S. Sujitjorn, K.-L. Areerak, and T. Kulworawanichpong, "The DQ axis with fourier (DQF) method for harmonic identification," *IEEE Transactions on Power Delivery*, vol. 22, no. 1, pp. 737–739, 2007.

[12] J. H. Xu, C. Lott, S. Saadate, and B. Davat, "Simulation and experimentation of a voltage source active filter compensating current harmonics and power factor," in *Proceedings of the 20th International Conference on Industrial Electronics, Control and Instrumentation*, pp. 411–415, Bologna, Italy, September 1994.

[13] L. Benchaita, S. Saadate, and A. Salem nia, "A comparison of voltage source and current source shunt active filter by simulation and experimentation," *IEEE Transactions on Power Systems*, vol. 14, no. 2, pp. 642–647, 1999.

[14] Y. Hayashi, N. Sato, and K. Takahashi, "A novel control of a current-source active filter for ac power system harmonic compensation," *IEEE Transactions on Industry Applications*, vol. 27, no. 2, pp. 380–385, 1991.

[15] S. Buso, L. Malesani, and P. Mattavelli, "Comparison of current control techniques for active filter applications," *IEEE Transactions on Industrial Electronics*, vol. 45, no. 5, pp. 722–729, 1998.

[16] M. P. Kazmierkowski and L. Malesani, "Current control techniques for three-phase voltage-source pwm converters: a survey," *IEEE Transactions on Industrial Electronics*, vol. 45, no. 5, pp. 691–703, 1998.

[17] W.-P. Zhou, D.-M. Liu, Z.-G. Wu, L. Xia, and X.-F. Yang, "The optimization-sliding mode control for three-phase three-wire DSP-based active power filter," in *Proceedings of the 5th International Power Electronics and Motion Control Conference (IPEMC '06)*, vol. 3, pp. 1680–1684, Shanghai, China, August 2006.

[18] J. Fei, T. Li, F. Wang, and W. Juan, "A novel sliding mode control technique for indirect current controlled active power filter," *Mathematical Problems in Engineering*, vol. 2012, Article ID 549782, 18 pages, 2012.

[19] N. Mendalek, F. Fnaiech, K. Al-Haddad, and L. Dessaint, "A non-linear optimal predictive control of a shunt active power filter," in *Proceedings of the 37th IAS Annual Meeting and World Conference on Industrial Applications of Electrical Energy*, pp. 70–77, Pittsburgh, Pa, USA, October 2002.

[20] A. M. Massoud, S. J. Finney, and B. W. Williams, "Predictive current control of a shunt active power filter," in *Proceedings of the IEEE 35th Annual Power Electronics Specialists Conference (PESC '04)*, pp. 3567–3572, Aachen, Germany, June 2004.

[21] M. Odavic, V. Biagini, P. Zanchetta, M. Sumner, and M. Degano, "One-sample-period-ahead predictive current control for high-performance active shunt power filters," *IET Power Electronics*, vol. 4, no. 4, pp. 414–423, 2011.

[22] P. Prasomsak, K.-L. Areerak, and A. Srikaew, "Control of shunt active power filters using fuzzy logic controller," in *Proceedings of the 30th IASTED Conference on Modelling, Identification, and Control (AsiaMIC '10)*, pp. 107–113, Phuket, Thailand, November 2010.

[23] J. Fei and S. Hou, "Adaptive fuzzy control with supervisory compensator for three-phase active power filter," *Journal of Applied Mathematics*, vol. 2012, Article ID 654937, 13 pages, 2012.

[24] N. Bruyant, M. Machmoum, and P. Chevrel, "Control of a three-phase active power filter with optimized design of the energy storage capacitor," in *Proceedings of the 29th Annual IEEE Power Electronics Specialists Conference (PESC '98)*, vol. 1, pp. 878–883, Fukuoka, Japan, May 1998.

[25] T. Narongrit, *Harmonic elimination using active power filter for balanced three-phase power system [M.S. thesis]*, Suranaree University of Technology, 2009.

[26] F. Mekri, B. Mazari, and M. Machmoum, "Control and optimization of shunt active power filter parameters by fuzzy logic," *Canadian Journal of Electrical and Computer Engineering*, vol. 31, no. 3, pp. 127–134, 2006.

[27] R. F. de Camargo and H. Pinheiro, "Three-phase four-wire shunt active filter to reduce voltage and current distortions in distribution systems," in *Proceedings of the 32nd Annual Conference on IEEE Industrial Electronics (IECON '06)*, pp. 1884–1889, Paris, France, November 2006.

[28] T. Narongrit, K.-L. Areerak, and K.-N. Areerak, "Current control of shunt active power filter using space vector PWM," in *Proceedings of the 9th International Conference on Electrical Engineering/Electronics, Computer, Telecommunications and Information Technology (ECTI-CON '12)*, pp. 1–4, Phetchaburi, Thailand, May 2012.

[29] W. Sheng, K. Liu, Y. Li, Y. Liu, and X. Meng, "Improved multiobjective harmony search algorithm with application to placement and sizing of distributed generation," *Mathematical Problems in Engineering*, vol. 2014, Article ID 871540, 8 pages, 2014.

[30] X. He and W. Wang, "Fuzzy multiobjective optimal power flow based on modified artificial BEE colony algorithm," *Mathematical Problems in Engineering*, vol. 2014, Article ID 961069, 12 pages, 2014.

[31] W. Haiquan, L. Liao, W. Dongyun, W. Shengjun, and D. Mingcong, "Improved artificial bee colony algorithm and its application in LQR controller optimization," *Mathematical Problems in Engineering*, vol. 2014, Article ID 695637, 8 pages, 2014.

[32] Z. Yan, C. Deng, B. Li, and J. Zhou, "Novel particle swarm optimization and its application in calibrating the underwater transponder coordinates," *Mathematical Problems in Engineering*, vol. 2014, Article ID 672412, 12 pages, 2014.

[33] I. S. Jesus and R. S. Barbosa, "Design of fuzzy fractional PD + I controllers tuned by a genetic algorithm," *Mathematical Problems in Engineering*, vol. 2014, Article ID 676121, 14 pages, 2014.

[34] D. Puangdownreong, K.-N. Areerak, A. Srikaew, S. Sujijorn, and P. Totarong, "System identification via adaptive Tabu search," in *Proceedings of the IEEE International Conference on Industrial Technology (ICIT '02)*, pp. 915–920, Bangkok, Thailand, 2002.

[35] T. Kulworawanichpong, K.-L. Areerak, K.-N. Areerak, and S. Sujitjorn, "Harmonic identification for active power filters via adaptive tabu search method," in *Knowledge-Based Intelligent Information and Engineering Systems*, vol. 3215 of *Lecture Notes in Computer Science*, pp. 687–694, Springer, Heidelberg, Germany, 2004.

[36] D. Puangdownreong, T. Kulworawanichpong, and S. Sujitjorn, "Input weighting optimization for PID controllers based on the adaptive tabu search," in *Proceedings of the IEEE Region 10 Conference on Analog and Digital Techniques in Electrical Engineering (TENCON '04)*, vol. 4, pp. 451–454, November 2004.

[37] D. Puangdownreong, K.-N. Areerak, K.-L. Areerak, T. Kulworawanichpong, and S. Sujitjorn, "Application of adaptive tabu search to system identification," in *Proceedings of the 24th IASTED International Conference on Modeling, Identification, and Control (MIC '05)*, pp. 178–183, Innsbruck, Austria, February 2005.

[38] R. Leepila, E. Oki, and N. Kishi, "Scheme to find k disjoint paths in multi-cost networks," in *Proceedings of the IEEE International Conference on Communications (ICC '11)*, pp. 1–5, Kyoto, Japan, June 2011.

[39] A. Oonsivilai and B. Marungsri, "Application of artificial intelligent technique for partial discharges localization in oil insulating transformer," *WSEAS Transactions on Systems*, vol. 7, pp. 920–929, 2008.

[40] T. Defeng, L. Shixing, X. Wujun, and Z. Yongming, "A fire monitoring system in ZigBee wireless network," in *Proceedings of the International Conference on Cyber-Enabled Distributed Computing and Knowledge Discovery (CyberC '10)*, pp. 48–51, Huangshan, China, October 2010.

[41] K. Chaijarurnudomrung, K.-N. Areerak, K.-L. Areerak, and A. Srikaew, "The controller design of three-phase controlled rectifier using an adaptive tabu search algorithm," in *Proceedings of the 8th International Conference on Electrical Engineering/Electronics, Computer, Telecommunications and Information Technology (ECTI-CON '11)*, pp. 605–608, Khon Kaen, Thailand, May 2011.

[42] J. Kluabwang, D. Puangdownreong, and S. Sujitjorn, "Multipath adaptive tabu search for a vehicle control problem," *Journal of Applied Mathematics*, vol. 2012, Article ID 731623, 20 pages, 2012.

[43] D. Puangdownreong, T. Kulworawanichpong, and S. Sujitjorn, "Finite convergence and performance evaluation of adaptive tabu search," in *Knowledge-Based Intelligent Information and Engineering Systems*, vol. 3215 of *Lecture Notes in Computer Science*, pp. 710–717, Springer, Heidelberg, Germany, 2004.

[44] T. Kulworawanichpong, D. Puangdownreong, and S. Sujitjorn, "Finite convergence of adaptive Tabu search," *ASEAN Journal on Science and Technology for Development*, vol. 21, no. 2-3, pp. 103–115, 2004.

[45] D. Puangdownreong, S. Sujitjorn, and T. Kulworawanichpong, "Convergence analysis of adaptive Tabu search," *Science Asia Journal of the Science Society of Thailand*, vol. 30, no. 2, pp. 183–190, 2004.

[46] S. Sujitjorn, J. Kluabwang, D. Puangdownreong, and N. Sarasiri, "Adaptive tabu search and management agent," *The ECTI Transactions on Electrical Engineering, Electronics, and Communications*, vol. 7, no. 2, pp. 1–10, 2009.

[47] S. Sujitjorn, T. Kulworawanichpong, D. Puangdownreong, and K.-N. Areerak, "Adaptive tabu search and applications in engineering design," in *Integrated Intelligent Systems for Engineering Design*, X. F. Zha and R. J. Howlett, Eds., pp. 233–257, IOS Press, Amsterdam, The Netherlands, 2006.